Published in final edited form as:
Neuroimage. 2011 October 15; 58(4): 1044–1050. doi:10.1016/j.neuroimage.2011.06.075.

A Whole-Brain Voxel Based Measure of Intrinsic Connectivity Contrast Reveals Local Changes in Tissue Connectivity with Anesthetic without A Priori Assumptions on Thresholds or Regions of Interest

Roberto Martuzzi[1,2], **Ramachandran Ramani**[3], **Maolin Qiu**[1], **Xilin Shen**[1], **Xenophon Papademetris**[1], and **R. Todd Constable**[1,4,5]

[1]Department of Diagnostic Radiology, Yale University School of Medicine, New Haven CT, USA [2]Laboratory of Cognitive Neuroscience, Brain-Mind Institute, Ecole Polytechnique Fédérale de Lausanne (EPFL) Lausanne, Switzerland [3]Department of Anesthesiology, Yale University School of Medicine, New Haven CT, USA [4]Department of Biomedical Engineering, Yale University School of Medicine, New Haven CT, USA [5]Department of Neurosurgery, Yale University School of Medicine, New Haven CT, USA

Abstract

The analysis of spontaneous fluctuations of functional magnetic resonance imaging (fMRI) signals has recently gained attention as a powerful tool for investigating brain circuits in a non-invasive manner. Correlation-based connectivity analysis investigates the correlations of spontaneous fluctuations of the fMRI signal either between a single seed region of interest (ROI) and the rest of the brain or between multiple ROIs. To do this, *a priori* knowledge is required for defining the ROI(s) and without such knowledge functional connectivity fMRI cannot be used as an exploratory tool for investigating the functional organization of the brain and its modulation under the different conditions. In this work we examine two indices that provide voxel based maps reflecting the intrinsic connectivity contrast (ICC) of individual tissue elements without the need for defining ROIs and hence require no *a priori* information or assumptions. These voxel based ICC measures can also be used to delineate regions of interest for further functional or network analyses. The indices were applied to the study of sevoflurane anesthesia-induced alterations in intrinsic connectivity. In concordance with previous studies, the results show that sevoflurane affects different brain circuits in a heterogeneous manner. In addition ICC analyses revealed changes in regions not previously identified using conventional ROI connectivity analyses, probably because of an inappropriate choice of the ROI in the earlier studies. This work highlights the importance of such voxel based connectivity methodology.

Address Correspondence to: Dr. R. Todd Constable Department of Diagnostic Radiology Yale University School of Medicine The Anlyan Center N-132 300 Cedar Street New Haven, CT 06520 todd.constable@yale.edu.

Introduction

The analysis of functional magnetic resonance imaging (fMRI) signals at rest has recently become a well-established and powerful tool for investigating specific brain circuits and states in a non-invasive manner. In their seminal work, Biswal *et al*. (1995) observed that at rest fluctuations in the blood oxygenation level dependent (BOLD) signals are correlated over time in different brain regions that belong to the same functional network. The origins of such correlations are thought to arise from synchronized neuronal activity between the regions (Fox and Raichle, 2007). These synchronous fluctuations of the BOLD signal have been demonstrated to be mostly confined in a very low-frequency band (Cordes et al., 2001; Lowe et al., 2000) and hence most of the work to-date, including the work presented here, has focused on low frequency (<0.1Hz) fluctuations.

The importance of resting state connectivity is not only related to the capability of highlighting the intrinsic organization of networks in the brain, but it is also related to the insight it provides into how such networks can be modulated by psychological or experimental conditions, medications, and disease. Indeed, there is increasing evidence linking connectivity to behavior (Hampson et al., 2006a; Hampson et al., 2006b) suggesting there may be a role in connectivity mapping for psychological profiling, and it has been shown to be altered in several clinical populations (Hoffman et al., 2007; Irwin et al., 2004; Lowe et al., 2002; Quigley et al., 2001; Saini et al., 2004; Waites et al., 2006). More recently, several studies have examined functional connectivity changes associated with the administration of anesthetic agents (Greicius et al., 2008; Kiviniemi et al., 2000; Kiviniemi et al., 2005; Martuzzi et al., 2010; Peltier et al., 2005), demonstrating heterogeneous changes across different functional networks and variations in the connectivity response associated with different drugs and doses.

Conventional connectivity analysis assesses correlations either between a single seed region of interest (ROI) and the rest of the brain or between multiple ROIs. While this approach is rapidly gaining widespread acceptance and has produced numerous insights into the functional organization of the brain, a fundamental weakness with this approach is that it requires the definition of at least one region of interest and in many studies several ROIs. That is, *a priori* knowledge is required to define the ROI(s) but *a priori* knowledge is not always available. There currently is no reliable means for defining ROIs throughout the cortex. In some regions, such as the hippocampus, it is relatively easy to define ROIs anatomically but anatomic definitions are extremely difficult in cortical regions such as the frontal and parietal lobes and even if ROIs can be defined in such regions they do not directly reflecting uniform function and thus are somewhat arbitrary. Atlas based definitions that rely on atlas's such as the Brodmann atlas are typically too large and therefore also not applicable. Finally, the use of task-based fMRI to define ROIs, while ideal in many ways, is limited by the number of tasks that can be run in a session and number of regions that tasks typically activate. Thus task-based definitions can lead to excellent ROI definitions but only in a very circumscribed set of regions that do not typically cover the whole-brain. This problem of ROI definition currently limits correlation based fc-fMRI use as an exploratory tool for data driven investigations into the brain regions that exhibit connectivity modulation under the different conditions such as investigations of CNS drug effects and phenotyping studies in genetics research.

To overcome the problem of defining and choosing ROIs, our group and others (Buckner et al., 2009; Constable et al., 2009a, b) have developed a whole-brain voxel based measure of connectivity, that uses network theory measures to represent how well connected any given voxel is to the rest of the gray matter voxels in the brain. The network measure of Degree (Rubinov and Sporns, 2010), represents the number of connections a given voxel has that

exceed a specific correlation threshold (normalized to fit a standard distribution). While this approach does not require *a priori* knowledge for the choice and the selection of the ROIs, it does require the definition of a correlation threshold to define the connected regions although these measures do not appear to be overly sensitive to the threshold chosen (Buckner et al., 2009).

In this work we, starting from the index defined by Buckner et al. (2009), we defined a novel index that takes into account not only the presence of a connection but also the strength of these connections, thereby producing voxel based maps reflecting the **intrinsic connectivity contrast** (ICC) of individual voxels without the need for defining any ROIs. This index has the advantage that it can be computed without applying a correlation threshold and therefore it does not require any *a priori* information or assumptions. ICC analysis was used to create a global picture of whether (and where) experimental manipulations modify the local connectivity pattern. We apply this measure to an anesthesia study contrasting data collected prior to and during the administration of sevoflurane anesthesia in healthy human volunteers. We test the hypothesis that anesthetic agents produce spatially non-uniform changes in the brain's underlying functional connections and that whole-brain voxel-based network measures can provide insight into the regional influence of an anesthetic agent on functional connectivity.

Theory

Two measures of network theory are defined to examine changes in the functional circuitry of the brain between the non-anesthetic and anesthetic state. The first measure, termed the *intrinsic connectivity contrast-degree* (ICC-d_{th}), is the measure of degree commonly used in network theory and previously used to investigate cortical hubs in Alzheimer's disease (Buckner et al., 2009) and epilepsy (Constable et al., 2009a, b). Given a certain threshold th, ICC-d_{th} at a voxel *i* can be expressed as in Eq. (1), where $r(i, j)$ is the connectivity value between voxels *i* an *j*, and $u(x)$ is the step function defined in Eq. (2).

$$\mathrm{ICC}-\mathrm{d}_{th}(i)=\sum_{j}u(|r(i,j)|-th),\quad i,j\in\text{brain} \tag{1}$$

$$u(x)=\begin{cases}0 & \text{if } x<0\\ 1 & \text{if } x>0\end{cases} \tag{2}$$

In other words, at a given reference voxel *i*, ICC-d_{th} represents the number of voxels in the brain that show a correlation with *i* above the threshold th (in absolute value). ICC-d_{th} is computed for each voxel in the brain, therefore producing a whole-brain map wherein the intensity of each voxel reflects the degree to which that voxel is connected to the rest of the brain. For statistical purposes, the values in the map are normalized to fit a Gaussian distribution with zero mean and unitary variance by subtracting the ICC-d_{th} obtained at each voxel by the average value across all the voxels and dividing this by the standard deviation of the whole-brain map (Buckner et al., 2009).

A second approach is to weight the connections with their r^2 value. We will call this second approach *intrinsic connectivity contrast-power* (ICC-p_{th}), and it is defined in Eq. (3).

$$\mathrm{ICC}-\mathrm{p}_{th}(i)=\sum_{j}r(i,j)^2\cdot u(|r(i,j)|-th),\quad i,j\in\text{brain} \tag{3}$$

Similarly to ICC-d_{th}, ICC-p_{th} values are normalized to fit a Gaussian distribution with zero mean and unitary variance. ICC-p_{th} represents the average r^2 connectivity of a given voxel *i* and all the other above-threshold voxels. While the computation of the degree map requires setting an arbitrary correlation threshold, the power map can be computed without the need for a correlation threshold, hence providing a metric that requires no *a priori* information either in terms of arbitrary thresholds or ROI definitions.

Materials and Methods

The data for these experiments has been previously published examining conventional ROI based connectivity changes between the non-anesthetic and anesthetic conditions (Martuzzi et al., 2010).

Subjects and experimental procedures

The study was conducted in 14 healthy ASA I (American Society of Anesthesiologists - physical status class I) subjects (7 male; 11 right and 3 left handed) in the age group of 22 to 34 years (mean age±SD 26.1±3 years). All subjects gave written informed consent and the study protocol was approved by the Human Investigation Committee of the Yale School of Medicine (New Haven, CT).

Subjects were interviewed and basic pre-anesthesia screening was carried out prior to the study, to ensure that they were eligible to participate in the study. Exclusion criteria included (but were not limited to) the use of psychoactive drugs or any centrally acting medication, history of epilepsy or renal disease, and presence of a potentially difficult airway. To prevent pulmonary aspiration of gastric contents (causing difficulty in breathing), all subjects fasted for 8 hours before the study and did not intake clear liquids for 2 hours prior to the experiment, as suggested in the ASA guidelines (ASA Task Force, 1999). During the experiment, lactated ringer was infused at 100 cc / hour to maintain infusion through a 22-gauge intravenous cannula for maintenance infusion and vital signs (EKG, non invasive blood pressure, pulse-oximeter and end-tidal carbon dioxide) were continuously monitored using an MR-compatible ASA monitor. Anesthesia was induced and maintained with a mixture of O_2 and 1% (end-tidal concentration) of sevoflurane, equivalent to 0.5 MAC[1] (minimum alveolar concentration), administered through a facemask held in place with head straps and connected to a semi-closed circle absorber circuit. Alveolar concentration of sevoflurane equilibrates with the concentration in the capillaries (arterial blood), which in turn equilibrates with brain tissue concentration. Measuring end tidal concentration of a volatile anesthetic like sevoflurane is a standard accepted practice in anesthesia. During the anesthesia period, the subjects were asleep, they did not respond to call, and had no memory of the event. Their Observer Assessment of Alertness and Sedation score (OAA/S; Chernik et al., 1990) was less than 3 on this scale ranging from 1 (fully anesthetized, i.e. subject does not respond even to prodding and nudging) to 5 (awake, i.e. subject responds readily to name calling in normal tone).

The study was comprised of three experimental sessions. In the first (pre-anesthesia) and last (post-anesthesia) sessions, pure oxygen was administrated to the subjects. In the second session (anesthesia), sevoflurane (0.5 MAC) was added to the pure oxygen. A 10 minute gap was introduced between experimental sessions to allow for end-tidal sevoflurane concentration to reach a steady state and to allow for anesthetic washout (respectively).

[1]0.5 MAC anesthesia refers to 50% of the concentration required for 1MAC. By definition, 1 MAC is the concentration required to suppress reflex motor response to a noxious stimulus in 50% of the subjects.

During the entire study, subjects were asked to lay in the scanner with their eyes closed and to refrain from performing any goal-oriented mental activity.

MR data acquisition

Images were acquired on a 3T Siemens (Erlangen, Germany) Trio MR system with a circularly polarized head coil. During each of the three experimental sessions (i.e. pre-anesthesia, anesthesia, and post-anesthesia), three functional runs of 210 volumes each were acquired using a T2*-sensitive gradient-recalled, single-shot echo-planar imaging pulse sequence (TR = 2 s, TE = 31 ms, FoV = 256 mm, flip angle 90°, matrix size 64×64). Each volume consisted of 33 slices parallel to the bicommissural plane (slice thickness 4mm, no gap).

To facilitate the anatomical registration across subjects, two additional anatomical volumes were acquired. First, a 2D T1-weighted sequence (TR = 300 ms, TE = 2.43 ms, FoV = 256 mm, matrix size 256×256, flip angle 60°) was acquired in the same position as the functional volumes using the same slice thickness and gap. Second, a 3D T1-weighted sagittal gradient-echo (MPRAGE) sequence was collected (176 contiguous sagittal slices, voxel size 1 mm^3, matrix size 256×256, FoV = 256 mm TR = 2530 ms, TE = 3.34 ms, flip angle = 7°).

Data Analysis

After discarding the first 10 volumes of each functional run (to allow for the magnetization to reach a steady state), data were slice-time and motion corrected using SPM5 (Wellcome Department of Cognitive Neurology, London, UK). At each voxel the BOLD signal was low-pass filtered with a 4^{th} degree elliptical filter (cut-off frequency: 0.08 Hz) and the 6 motion parameters, the mean signals of white matter and CSF, and linear and quadratic drifts were regressed from the data (Laufs et al., 2007). For each individual, white matter and CSF masks were obtained by first segmenting the MPRAGE and than transforming the segmented maps into the space of the functional images. The mean white matter and CSF signals were computed by extracting the average BOLD signals within these masks and finally, for each slice independently the mean slice time course was removed. For each of the experimental conditions (i.e. pre-anesthesia, anesthesia, and post-anesthesia) the three functional runs were concatenated after the removal of the mean value and the degree measure was computed applying a correlation threshold of 0.25, and the degree power ICC map was also computed without applying a threshold.

To facilitate group statistics, single subject results were normalized to the MNI standard template using the intensity-only component of the method reported in Papademetris et al. (2004), and implemented within the BioImage Suite software package (www.bioimagesuite.org). First, the EPI images were linearly coregistered to the individual co-localized T1 2D slices. This T1 2D volume was then linearly registered to that subject's 3D volume acquisition. The combination of these two transformations matrix was applied to the ICC maps. The individual subject's 3D was then registered to the MNI brain using both linear and nonlinear registration steps in BioimageSuite.org and the same transformation matrix was again applied to the single subject ICC maps.

Group analyses were carried out as a second level of statistic. Differences between pre-anesthesia and anesthesia ICC maps were identified using a paired t-test ($p<0.005$ uncorrected, 5-voxel cluster threshold; resulting in $p<0.05$ uncorrected at cluster level). Regions with reliable ICC differences between the two experimental sessions were anatomically identified using the Talairach Daemon Atlas (Lancaster et al., 2000), after

transforming MNI coordinates into Talairach coordinates corrected using a non-linear transformation (Lacadie et al., 2008).

For selected nodes highlighted by the ICC results, follow up ROI analysis was conducted using classical fc-fMRI investigation with the nodes as seed regions. Briefly, for each subject the average signal of the ROI was computed and correlated with the signal extracted within each voxel in the brain. To compute group results, correlation values were first transformed into Gaussian values by means of the Fisher transform, single-subject maps were then normalized to the standard MNI template, and the null hypothesis across pre- and post-ansesthesia conditions was assessed using a paired t-test. Details on this method can be found elsewhere (Martuzzi et al., 2010).

Results

A previous study based on the same data (Martuzzi et al., 2010) showed little change between the pre- and post- anesthesia conditions for BOLD activation data. Consistently with that results, pre- versus post-anesthesia ICC comparison highlighted small and sparse clusters, which confirmed the hypothesis of a almost complete washout of the anesthetic drug during the 10 minutes following the end of the sevoflurane administration. A complete listing of these clusters is reported in Table S1 of the Supplementary materials.

During the MR session, heart and respiratory rates, blood pressure, end-tidal CO_2, and O_2 partial pressure (SpO_2) were constantly monitored. The comparison of these parameters between the pre-anesthesia and anesthesia conditions revealed that the administration of sevoflurane induced statistically significant changes only in systolic (pre-anesthesia: 114±9.2 mmHg, anesthesia: 109±7.0 mmHg, $p = 0.002$), diastolic (pre-anesthesia: 68±5.3 mmHg, anesthesia: 63±5.2 mmHg, $p = 0.019$), and mean blood pressure (pre-anesthesia: 83±6.2 mmHg, anesthesia: 78±5.2 mmHg, $p = 0.008$). Heart rate, respiratory rates, SpO_2, and end-tidal CO_2 did not show significant change ($p > 0.1$) with 0.5 MAC sevoflurane anesthesia.

The analysis of the differences in intrinsic connectivity between the periods prior to and during anesthesia administration revealed that sevoflurane influences functional connectivity in a heterogeneous manner, decreasing the overall connectivity in some areas and increasing it in others. The results of the analysis of the ICC-$d_{0.25}$ are shown in Fig. 1a and Table 1. This analysis revealed an increase in the connectivity of the primary motor cortex, the supplementary motor area (SMA), the posterior insula, and the extrastriate visual cortex (BA 18/19), as well as in the superior temporal gyrus bilaterally. Conversely, in the right superior frontal gyrus (BA 6), in a portion of the posterior cingulated cortex (PCC), in the posterior part of the left middle temporal gyrus (BA 37), in the secondary somatosensory cortex (SII; BA40), and in several portions of the cerebellum the connectivity was reduced during sevoflurane administration. Because the increase in the connectivity in the insula was not predicted on the basis of previous results where the entire insula was used as seed region, follow-up analyses were conducted using classical fc-fMRI methods using the two sections of the insula highlighted in the ICC-$d_{0.25}$ results as seeds regions. Both these analyses (one per ROI) showed an increase in connectivity to the thalamus bilaterally (See Fig. 2).

Analysis using the ICC-$p_{0.25}$ measure showed similar results to those obtained using the degree maps (See Fig. 1b and Table 2), indicating that these two measures carry similar information, although the ICC-p demonstrated slightly less sensitivity. For example the analysis of ICC-$p_{0.25}$ did not reveal connectivity changes in the primary motor cortex, as highlighted by the ICC-$d_{0.25}$. The computation of the ICC power however does not require the choice of a threshold in the connectivity measures. Indeed, other than the slight decrease

in sensitivity, analyzing the power map when no threshold is applied (e.g. ICC-$p_{0.00}$), highlights the same regions observed in the measures obtained with an arbitrary threshold of 0.25 in place (ICC-$p_{0.25}$ and ICC-$d_{0.25}$).

Discussion

The aim of this paper was to introduce a novel network theory approach – intrinsic connectivity contrast (ICC) – to evaluate variations in connectivity properties at the level of individual voxels without the need for predefining ROIs. Previously, Buckner et al. (2009) presented this approach as a method for isolating hubs for further network analysis in Alzheimer's disease. The ICC-power approach introduced here takes into account not only the number of connections between one voxel and the rest of the brain, but also the strength of these connections and in this way can be applied without the need to assign an arbitrary correlation threshold in order to identify which brain region exhibit changes in their overall functional connectivity. The identified regions can then be used as ROI in a classical fc-fMRI analysis to identify which connections of that particular node are affected by the experimental manipulations.

ICC values represent either the number of connections (ICC-d) or the average strength of these connections (ICC-p) between a given voxel and the rest of the brain. Variations in this measure between different experimental conditions (or across patient populations) highlight the tissue elements in the brain that exhibit altered connectivity as a function of condition (or population). These new indices provide explorative tools to localize changes in functional connectivity related to experimental modulations and/or groups. Classical ROI based fMRI connectivity analysis on the regions exhibiting local changes can then be performed to understand the networks associated with the identified nodes.

An alternative way to explore changes in functional connectivity is to parcellate the cerebral cortex according to either functional or anatomical atlas and to run multiple fc-fMRI analyses using each parcel as a seed region. Anatomic parcellation of the cortex would allow a complete exploration of brain connectivity and of its changes but it relies on the assumption that anatomic parcellations include unique functional subunits within each region. If this assumption is false, as is likely the case in many regions, then the average time-course for an ROI may not be representative of the time-courses of any of the functional subunits within that ROI and the connectivity measured will therefore be meaningless. Such anatomic parcellation has been used (see Hagman *et al*. (2008) or Honey *et al*. (2009)) with up to 998 anatomically defined ROIs. In those papers the focus was on examining the relationship between structure and function for only the nodes exhibiting the strongest connectivity and while not explicitly examined, these may well have been nodes where the anatomic parcellation happened to line up nicely with function. In fact using resting-state data to parcellate individual functional subunits within larger ROIs is a growing area of research (see for example (Shen et al., 2010)). The voxel based measure of degree employed in this work circumvents the initial parcellation problem by operating at the level of voxels.

In this paper we employed two indices of ICC using a previously published dataset in which functional connectivity changes induced by sefoflurane administration were examined.

Under anesthesia, a significant drop in blood pressure (systolic, diastolic and mean) was observed. However, functional MR images were acquired 10 minutes after the begining of sevoflurane administration to allow for end-tidal sevoflurane concentration to reach a steady state, therefore avoiding transient effects. With this precaution, the blood pressure remained stable during the entire acquisition period under anesthesia. The drop in arterial pressure is

not likely to influence CBF and BOLD signal, because under sevoflurane the arterial pressure is still within the range of autoregulation for the brain (60–160 mm/hg) and under stable or slow varying blood pressure conditions the CBF does not change with change in blood pressure within the range of autoregulation (Zaharchuk et al., 1999). Thus we do not expect that changes in blood pressure influenced the BOLD signal results shown. Additionally, the calculation of ICC involves calculation of the correlation coefficient between BOLD time courses and this coefficient, when not dominated by noise, is independent of the magnitude of the BOLD time courses, again suggesting that a change in blood pressure would not influence the calculated ICC values.

Consistent with the previous paper (Martuzzi et al., 2010) the comparison between the pre- and post-anesthesia periods revealed a few significant clusters, indicating that the two conditions were not completely identical. However, all the clusters observed in this pre- and post- anesthesia period contrast, while close to the accepted level of significance, none of them was co-localized with the clusters showing differences between pre- and anesthesia periods. These two observations suggest that these differences are unlikely to be related to long-lasting effects of the anesthetic agent, but may be related to the increased subject discomfort as the anesthesia state was reversed.

In our previous paper (Martuzzi et al., 2010) we interrogated specific ROIs, including the thalamus, the primary motor, auditory, and visual cortices, the insula, the hippocampus, and the PCC. This analysis revealed that sevoflurane anesthesia decreases the connectivity between the hippocampus and PCC and bilateral inferior parietal lobule (IPL), and increases that between insula and SII, while affects the connectivity of the thalamus in an heterogeneous way, increasing it with some structure (i.e. the supplementary motor area and portions of the insula) and decreasing with others (i.e. the caudate and the left IPL). The results of ICC analysis mostly replicated these previous results that interrogated specific ROIs, such as modulation of the connectivity in SII and in part of the PCC, but in this case without the need to define seed regions ahead of time. In addition, the new analysis highlighted changes in the superior frontal gyrus and middle temporal gyrus that were not previously observed due to a lack of a priori knowledge on how to properly define the seed ROIs in this region.

There are two explanations for increased connectivity within the posterior insula. First, the ICC indices measure the total connectivity between a single voxel and all of its other connections. Thus while there may be decreased connectivity between the insula and SII the insula is connected to many regions (Augustine, 1996) and increases in these other connections could out-weigh the decrease with SII. Indeed, the follow up analysis conducted using classical fc-fMRI methods revealed that the ICC increase in the insula is mostly due to an increase in the connectivity between that specific region of the insula and the thalamus. Second, ROI analysis identifies only the connectivity patterns that can be observed relative to the mean ROI signal. This implicitly assumes that the mean ROI time-course is representative of the ROI as a whole. However it may not be representative of individual elements within the ROI if the ROI is made up of multiple independent functional subunits The ICC approach described here has revealed that the administration of sevoflurane does not modulate the connectivity of the insula homogeneously and this is a finding that would not have been apparent examining an ROI encompassing the entire insula. Nevertheless the disparate findings between ROI based connectivity and ICC in these instances highlight the different types of information provided by these analyses.

The small ICC changes observed in the low sensory cortex and the decreases observed in the superior frontal and middle temporal gyri as well as in SII is consistent with the view that

sevoflurane at 0.5 MAC preferentially reduces the connections of regions involved in higher order functions (Martuzzi et al., 2010) at this low dose.

The study reported here highlights the importance of having a whole-brain voxel based measure of functional connectivity that can be used as an exploratory tool for investigating functional changes induced by drug administration or by a particular disease. These voxel based ICC measures can also be used (as in Buckner et al., 2009) to delineate regions of interest for further functional or network analyses. By moving to a voxel level we are implicitly using as fine a parcellation of the cortex as allowed with the given acquisition strategy. Ideally, we would prefer to have an atlas of individual functional subunits (as described in Shen et al., 2010) that are larger than a single voxel but not as large as the Brodmann areas and contain a uniform functional subunit that is more meaningful for this type of analysis than a Brodmann or an anatomic atlas. Such an atlas of functional subunits would yield results very similar to those found here with a voxel based strategy but with more statistical power, and hence more sensitivity, due to the reduced number of multiple comparisons and noise reduction effects of combining voxel time-courses in a meaningful way. However, to date such an atlas does not yet exist.

In summary, in this work we have presented a new whole-brain voxel based index that allows the investigation of changes in functional connectivity, without the need for any *a priori* information – e.g. choice of the seed region or arbitrary connectivity threshold. This new index was applied to the study of anesthesia-induced alterations in intrinsic connectivity, revealing changes in regions that were not previously identified in conventional ROI connectivity analyses; therefore highlighting the importance of such an exploratory methodology.

Supplementary Material

Refer to Web version on PubMed Central for supplementary material.

Acknowledgments

We thank Karen Martin for technical assistance. This material is based on work supported by the National Institutes of Health (NIH) R01 NS052344-04

References

Augustine JR. Circuitry and functional aspects of the insular lobe in primates including humans. Brain Res Brain Res Rev. 1996; 22:229–244. [PubMed: 8957561]

Biswal B, Yetkin FZ, Haughton VM, Hyde JS. Functional connectivity in the motor cortex of resting human brain using echo-planar mri. Magnetic Resonance in Medicine. 1995; 34:537–541. [PubMed: 8524021]

Buckner RL, Sepulcre J, Talukdar T, Krienen FM, Liu H, Hedden T, Andrews-Hanna JR, Sperling RA, Johnson KA. Cortical Hubs Revealed by Intrinsic Functional Connectivity: Mapping, Assessment of Stability, and Relation to Alzheimer's Disease. J. Neurosci. 2009; 29:1860–1873. [PubMed: 19211893]

Constable RT, Hara Y, Tokoglu F, Papademetris X. Intrinsic connectivity contrast: A novel contrast mechanism for investigating a wide range of brain disorders. Proceedings of the ISMRM Annual Meeting, Hawaii. 2009a; 17:4493.

Constable, RT.; Hara, Y.; Tokoglu, F.; Papademetris, X. Intrinsic Connectivity Contrast: A voxel level summary of tissue connectivity. Proceedings of the OHBM 15th Annual Meeting; 2009b. p. 275-M

Cordes D, Haughton VM, Arfanakis K, Carew JD, Turski PA, Moritz CH, Quigley MA, Meyerand ME. Frequencies Contributing to Functional Connectivity in the Cerebral Cortex in “Resting-state” Data. AJNR Am J Neuroradiol. 2001; 22:1326–1333. [PubMed: 11498421]

Fox MD, Raichle ME. Spontaneous fluctuations in brain activity observed with functional magnetic resonance imaging. Nat Rev Neurosci. 2007; 8:700–711. [PubMed: 17704812]

Greicius MD, Kiviniemi V, Tervonen O, Vainionpää V, Alahuhta S, Reiss AL, Menon V. Persistent default-mode network connectivity during light sedation. Human Brain Mapping. 2008; 29:839–847. [PubMed: 18219620]

Hagmann P, Cammoun L, Gigandet X, Meuli R, Honey CJ, Wedeen VJ, Sporns O. Mapping the structural core of human cerebral cortex. PLoS Biol. 2008; 6:e159. [PubMed: 18597554]

Hampson M, Driesen NR, Skudlarski P, Gore JC, Constable RT. Brain Connectivity Related to Working Memory Performance. J. Neurosci. 2006a; 26:13338–13343. [PubMed: 17182784]

Hampson M, Tokoglu F, Sun Z, Schafer RJ, Skudlarski P, Gore JC, Constable RT. Connectivity-behavior analysis reveals that functional connectivity between left BA39 and Broca's area varies with reading ability. Neuroimage. 2006b; 31:513–519. [PubMed: 16497520]

Hoffman RE, Hampson M, Wu K, Anderson AW, Gore JC, Buchanan RJ, Constable RT, Hawkins KA, Sahay N, Krystal JH. Probing the pathophysiology of auditory/verbal hallucinations by combining functional magnetic resonance imaging and transcranial magnetic stimulation. Cereb Cortex. 2007; 17:2733–2743. [PubMed: 17298962]

Honey CJ, Sporns O, Cammoun L, Gigandet X, Thiran JP, Meuli R, Hagmann P. Predicting human resting-state functional connectivity from structural connectivity. Proceedings of the National Academy of Sciences. 2009; 106:2035–2040.

Irwin W, Anderle MJ, Abercrombie HC, Schaefer SM, Kalin NH, Davidson RJ. Amygdalar interhemispheric functional connectivity differs between the non-depressed and depressed human brain. NeuroImage. 2004; 21:674–686. [PubMed: 14980569]

Kiviniemi V, Jauhiainen J, Tervonen O, Pääkkö E, Oikarinen J, Vainionpää V, Rantala H, Biswal B. Slow vasomotor fluctuation in fMRI of anesthetized child brain. Magnetic Resonance in Medicine. 2000; 44:373–378. [PubMed: 10975887]

Kiviniemi VJ, Haanpää H, Kantola J-H, Jauhiainen J, Vainionpää V, Alahuhta S, Tervonen O. Midazolam sedation increases fluctuation and synchrony of the resting brain BOLD signal. Magnetic Resonance Imaging. 2005; 23:531–537. [PubMed: 15919598]

Lacadie CM, Fulbright RK, Rajeevan N, Constable RT, Papademetris X. More accurate Talairach coordinates for neuroimaging using non-linear registration. Neuroimage. 2008; 42:717–725. [PubMed: 18572418]

Lancaster JL, Woldorff MG, Parsons LM, Liotti M, Freitas CS, Rainey L, Kochunov PV, Nickerson D, Mikiten SA, Fox PT. Automated Talairach Atlas labels for functional brain mapping. Human Brain Mapping. 2000; 10:120–131. [PubMed: 10912591]

Laufs H, Walker MC, Lund TE. 'Brain activation and hypothalamic functional connectivity during human non-rapid eye movement sleep: an EEG/fMRI study'--its limitations and an alternative approach. Brain. 2007; 130:e75. [PubMed: 17584775]

Lowe MJ, Dzemidzic M, Lurito JT, Mathews VP, Phillips MD. Correlations in Low-Frequency BOLD Fluctuations Reflect Cortico-Cortical Connections. Neuroimage. 2000; 12:582–587. [PubMed: 11034865]

Lowe MJ, Phillips MD, Lurito JT, Mattson D, Dzemidzic M, Mathews VP. Multiple sclerosis: low-frequency temporal blood oxygen level-dependent fluctuations indicate reduced functional connectivity initial results. Radiology. 2002; 224:184–192. [PubMed: 12091681]

Martuzzi R, Ramani R, Qiu M, Rajeevan N, Constable RT. Functional connectivity and alterations in baseline brain state in humans. NeuroImage. 2010; 49:823–834. [PubMed: 19631277]

Papademetris, X.; Jackowski, AP.; Schultz, RT.; Staib, LH.; Duncan, JS. Medical Image Computing and Computer-Assisted Intervention – MICCAI 2004. 2004. Integrated Intensity and Point-Feature Nonrigid Registration; p. 763-770.

Peltier SJ, Kerssens C, Hamann SB, Sebel PS, Byas-Smith M, Hu X. Functional connectivity changes with concentration of sevoflurane anesthesia. Neuroreport. 2005; 16:285–288. [PubMed: 15706237]

Quigley M, Cordes D, Wendt G, Turski P, Moritz C, Haughton V, Meyerand ME. Effect of focal and nonfocal cerebral lesions on functional connectivity studied with MR imaging. AJNR Am J Neuroradiol. 2001; 22:294–300. [PubMed: 11156772]

Rubinov M, Sporns O. Complex network measures of brain connectivity: uses and interpretations. NeuroImage. 2010; 52:1059–1069. [PubMed: 19819337]

Saini S, DeStefano N, Smith S, Guidi L, Amato MP, Federico A, Matthews PM. Altered cerebellar functional connectivity mediates potential adaptive plasticity in patients with multiple sclerosis. J Neurol Neurosurg Psychiatry. 2004; 75:840–846. [PubMed: 15145996]

Shen X, Papademetris X, Constable RT. Graph-theory based parcellation of functional subunits in the brain from resting-state fMRI data. Neuroimage. 2010; 50:1027–1035. [PubMed: 20060479]

Waites AB, Briellmann RS, Saling MM, Abbott DF, Jackson GD. Functional connectivity networks are disrupted in left temporal lobe epilepsy. Ann Neurol. 2006; 59:335–343. [PubMed: 16404743]

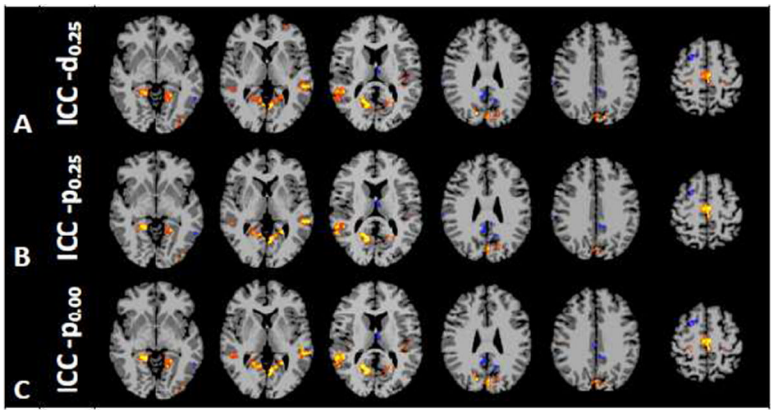

Figure 1.

Significant ICC-$d_{0.25}$ (A), ICC-$p_{0.25}$ (B), and ICC-$p_{0.00}$ (C) contrasts between anesthesia and pre-anesthesia periods within different axial slices shown in radiological Anesthesia changes heterogeneously the connectivity in the brain, increasing the connectivity in the primary motor cortex, in the supplementary motor area (SMA), in the posterior insula, and in the extrastriate visual cortex (BA 18/19), as well as in the superior temporal gyrus bilaterally, and decreasing it in the right superior frontal gyrus (BA 6), in portion of the posterior cingulated cortex (PCC), in the posterior part of the left middle temporal gyrus (BA 37), in the secondary somatosensory cortex (SII; BA40), and in several portions of the cerebellum.

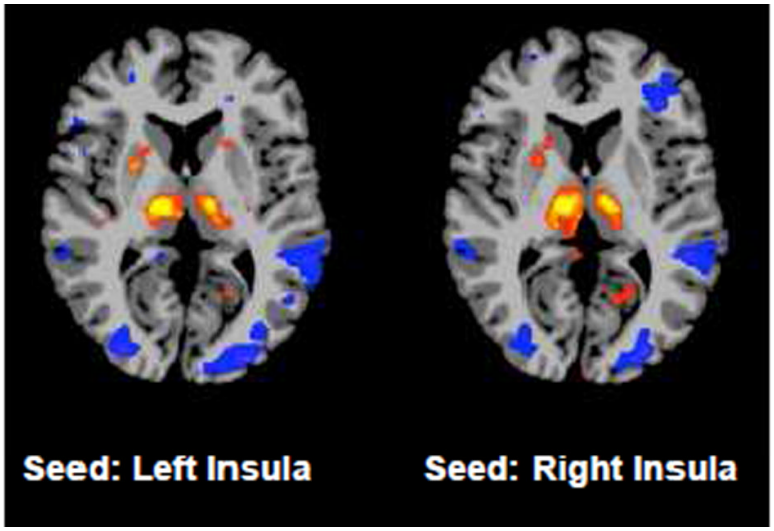

Figure 2.
Results of the follow-up analysis using the right and left insula clusters as seeds regions ($p<0.005$). Results show that the increase in ICC is mostly due to an increased connectivity between that portion of the insula and the thalamus, bilaterally.

Table 1

Regions showing significant different values in the ICC-d25 between the pre- and the anesthesia periods

MNI coord (mm)			Talairach coord (mm)			T values	Cluster size		Brain region	Broadman Area
x	y	z	x	y	z					
Positive clusters										
15	−75	27	15	−72	26	8.82	7	R	Precuneus	BA 31
−3	−84	30	−3	−80	29	8.02	71	L	Cuneus	BA 18
18	−57	9	18	−55	12	6.44	203	R	Posterior Cingulate	BA 30
−54	−36	3	−51	−36	6	6.11	33	L	Middle Temporal Gyrus	BA 22
−24	−57	9	−23	−56	12	5.87	146	L	Posterior Cingulate	BA 30
48	−45	12	47	−44	14	5.83	79	R	Superior Temporal Gyrus	BA 13
−12	−81	36	−12	−77	34	5.76	30	L	Cuneus	BA 19
−48	−24	15	−46	−24	16	5.45	65	L	Insula	BA 41
0	−27	60	0	−23	54	5.39	102	L	Medial Frontal Gyrus	BA 6
−39	−87	−6	−39	−85	0	5.32	22	L	Inferior Occipital Gyrus	BA 18
−39	−21	45	−39	−19	42	5.3	11	L	Precentral Gyrus	BA 4
42	−36	18	41	−35	19	4.33	32	R	Insula	BA 13
24	−36	60	25	−32	54	4.33	5	R	Postcentral Gyrus	BA 3
−18	−30	63	−18	−26	57	4.02	18	L	Precentral Gyrus	BA 4
−30	51	6	−30	48	5	3.98	8	L	Middle Frontal Gyrus	BA 10
24	−30	57	25	−26	52	3.82	8	R	Precentral Gyrus	BA 4
Negative clusters										
24	6	57	24	9	52	6.5	15	R	Superior Frontal Gyrus	BA 6
−3	−9	9	−2	−10	11	5.03	19	L	Thalamus	
−57	−57	−6	−54	−57	0	4.97	10	L	Middle Temporal Gyrus	BA 37
−15	−57	24	−14	−55	24	4.78	9	L	Cingulate Gyrus	BA 31
−33	30	45	−32	31	41	4.72	9	L	Middle Frontal Gyrus	BA 8
66	−27	27	64	−26	27	4	8	R	Inferior Parietal Lobule	BA 40
3	−45	27	3	−43	27	3.9	15	R	Cingulate Gyrus	BA 31
−6	−45	33	−5	−43	32	3.84	9	L	Cingulate Gyrus	BA 31

Neuroimage. Author manuscript; available in PMC 2012 October 15.

Table 2

Regions showing significant different values in the ICC-p25 between the pre- and the anesthesia periods

MNI coord (mm)			Talairach coord (mm)			T values	Cluster size		Brain region	Broadman Area
x	y	z	x	y	z					
Positive clusters										
12	−63	15	12	−61	17	6.7	187	R	Posterior Cingulate	BA 31
−63	−36	3	−59	−36	7	5.89	27	L	Middle Temporal Gyrus	BA 22
−48	−24	15	−46	−24	16	5.57	39	L	Insula	BA 41
−24	−57	9	−23	−56	12	5.55	108	L	Posterior Cingulate	BA 30
54	−54	9	54	−53	12	5.44	66	R	Superior Temporal Gyrus	BA 39
−3	−84	30	−3	−80	29	5.35	62	L	Cuneus	BA 18
0	−27	60	0	−23	54	5.21	102	L	Medial Frontal Gyrus	BA 6
−12	−81	36	−12	−77	34	5.07	23	L	Cuneus	BA 19
−39	−87	−6	−39	−85	0	4.63	19	L	Inferior Occipital Gyrus	BA 18
45	−21	36	44	−19	34	4.58	13	R	Precentral Gyrus	BA 4
−12	−66	15	−11	−64	16	4.56	12	L	Posterior Cingulate	BA 31
15	−75	27	15	−72	26	4.52	5	R	Precuneus	BA 31
−39	−21	45	−39	−19	42	4.51	7	L	Precentral Gyrus	BA 4
33	−24	15	32	−24	16	4.16	28	R	Insula	BA 13
3	−63	3	3	−61	7	4.08	5	R	Posterior Cingulate	BA 30
Negative clusters										
24	6	57	24	9	52	5.3	6	R	Superior Frontal Gyrus	BA 6
−3	−9	9	−2	−10	11	5	19	L	Thalamus	
−57	−57	−6	−54	−57	0	4.77	15	L	Middle Temporal Gyrus	BA 37
30	21	54	30	24	50	4.45	12	R	Superior Frontal Gyrus	BA 8
−12	−57	27	−11	−54	27	4.44	9	L	Cingulate Gyrus	BA 31
66	−27	27	64	−26	27	4.09	9	R	Inferior Parietal Lobule	BA 40
−12	−45	33	−11	−43	32	4.02	11	L	Cingulate Gyrus	BA 31
3	−45	27	3	−43	27	3.94	10	R	Cingulate Gyrus	BA 31
0	−42	33	0	−40	32	3.46	5	L	Cingulate Gyrus	BA 31

Table 3

Regions showing significant different values in the ICC-p00 between the pre- and the anesthesia periods

MNI coord (mm)			Talairach coord (mm)			T values	Cluster size		Brain region	Broadman Area
x	y	z	x	y	z					
Positive clusters										
−3	−84	30	−3	−80	29	6.79	67	L	Cuneus	BA 18
18	−57	9	18	−55	12	6.61	201	R	Posterior Cingulate	BA 30
15	−75	27	15	−72	26	6.43	8	R	Precuneus	BA 31
−48	−24	15	−46	−24	16	6.28	67	L	Insula	BA 41
51	−42	9	50	−41	12	6.19	80	R	Middle Temporal Gyrus	BA 21
−6	−63	3	−5	−61	6	5.65	131	L	Posterior Cingulate	BA 30
−54	−30	0	−51	−31	4	5.51	35	L	Superior Temporal Gyrus	BA 22
−6	−18	57	−5	−15	52	5.43	106	L	Medial Frontal Gyrus	BA 6
−39	−21	45	−39	−19	42	5.42	13	L	Precentral Gyrus	BA 4
−12	−81	36	−12	−77	34	5.01	26	L	Cuneus	BA 19
45	−21	36	44	−19	34	4.84	14	R	Precentral Gyrus	BA 4
−12	−66	15	−11	−64	16	4.55	14	L	Posterior Cingulate	BA 31
33	−24	15	32	−24	16	4.54	31	R	Insula	BA 13
−39	−87	−6	−39	−85	0	4.41	19	L	Inferior Occipital Gyrus	BA 18
−18	−30	63	−18	−26	57	4.14	23	L	Precentral Gyrus	BA 4
48	−60	0	48	−60	4	3.67	6	R	Middle Temporal Gyrus	BA 37
Negative clusters										
−6	−45	78	−5	−40	69	6.72	6	L	Postcentral Gyrus	BA 5
24	6	57	24	9	52	6.47	10	R	Superior Frontal Gyrus	BA 6
−3	−9	9	−2	−10	11	5.27	23	L	Thalamus	
−57	−57	−6	−54	−57	0	4.59	8	L	Middle Temporal Gyrus	BA 37